Article

Green, Solvent-Free Mechanochemical Synthesis of Nano Ag₂O/MnO₂/N-Doped Graphene Nanocomposites: An Efficient Catalyst for Additive-Base-Free Aerial Oxidation of Various Kinds of Alcohols

Mohammad Rafe Hatshan, Mujeeb Khan, Mohamed E. Assal, Mohammed Rafi Shaik, Mufsir Kuniyil, Abdulrahman Al-warthan, Mohammed Rafiq H. Siddiqui, and Syed Farooq Adil*

Read Online

ACCESS | Metrics & More | Article Recommendations | SI Supporting Information

ABSTRACT: Herein, we report a solvent-less, straightforward, and facile mechanochemical technique to synthesize nanocomposites of Ag₂O nanoparticles-doped MnO₂, which is further codoped with nitrogen-doped graphene (N-DG) [i.e., (X %)N-DG/MnO₂−(1% Ag₂O)] using physical milling of separately prepared N-DG and Ag₂O NPs−MnO₂ annealed at 400 °C over an eco-friendly ball-mill process. To assess the efficiency in terms of catalytic performance of the nanocomposites, selective oxidation of benzyl alcohol (BlOH) to benzaldehyde (BlCHO) is selected as a substrate model with an eco-friendly oxidizing agent (O₂ molecule) and without any requirements for the addition of any harmful additives or bases. Various nanocomposites were prepared by varying the amount of N-DG in

the composite, and the results obtained highlighted the function of N-DG in the catalyst system when they are compared with the catalyst MnO₂−(1% Ag₂O) [i.e., undoped catalyst] and MnO₂−(1% Ag₂O) codoped with different graphene dopants such as GRO and H-RG for alcohol oxidation transformation. The effects of various catalytic factors are systematically evaluated to optimize reaction conditions. The N-DG/MnO₂−(1% Ag₂O) catalyst exhibits premium specific activity (16.0 mmol/h/g) with 100% BlOH conversion and <99.9% BlCHO selectivity within a very short interval. The mechanochemically prepared N-DG-based nanocomposite displayed higher catalytic efficacy than that of the MnO₂−(1% Ag₂O) catalyst without the graphene dopant, which is N-DG in this study. A wide array of aromatic, heterocyclic, allylic, primary, secondary, and aliphatic alcohols have been selectively converted to respective ketones and aldehydes with full convertibility without further oxidation to acids over N-DG/MnO₂−(1% Ag₂O). Interestingly, it is also found that the N-DG/MnO₂−(1% Ag₂O) can be efficiently reused up to six times without a noteworthy decline in its effectiveness. The prepared nanocomposites were characterized using various analytical, microscopic, and spectroscopic techniques such as X-ray diffraction, thermogravimetric analysis, Fourier-transform infrared spectroscopy, Raman, field emission scanning electron microscopy, and Brunauer−Emmett−Teller.
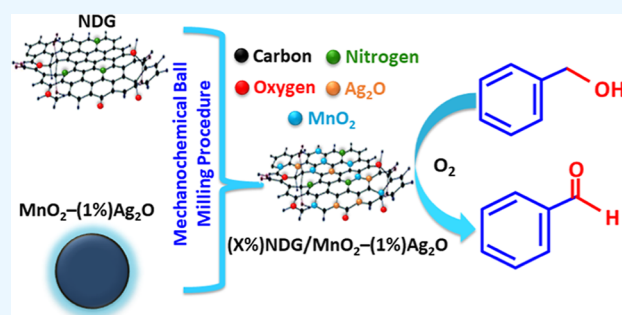
1. INTRODUCTION

Catalytic oxidation of alcohols to produce respective carbonyl compounds (i.e., aldehydes and ketones) is one of the most pivotal and valuable organic reactions in synthetic chemistry from an industrial and scientific viewpoint.[1] These transformations have received increasing interest, attributed to the numerous applications of carbonyls in the industries of plastics, insecticides, dyes, flame retardants, cosmetics, and pharmaceuticals.[2] In conventional procedures, stoichiometric oxidizing agents, such as dichromate, hypochlorite, permanganate, and chromium oxide, are used. These oxidants are expensive, poisonous, and generate enormous amounts of heavy metal waste and hazardous byproducts.[3] With growing environmental concerns, it is necessary to replace undesirable classically stoichiometric processes with more environmentally benign methodologies using molecular O₂ or air as a green oxidant in order to reduce ecologically unacceptable wastes.[4] In most cases,

heterogeneous catalysts are preferred to homogeneous ones in industrial chemistry owing to their recyclability, low toxicity, ease of storage, and tolerance for harsh conditions (e.g., high pressure and temperatures).[5] In this context, noble metallic NPs (such as Au, Pd, Ru, and Pt) have been extensively employed as oxidation catalysts with high efficiency. Although these catalysts usually have some drawbacks, including low abundance, high toxicity, and cost.[6] Therefore, significant efforts are being made to develop low-cost and abundant catalysts such as transition

Scheme 1. Preparation of N-DG/MnO$_2$−(1% Ag$_2$O) Nanocomposites via a Mechanochemical Ball-Milling Procedure
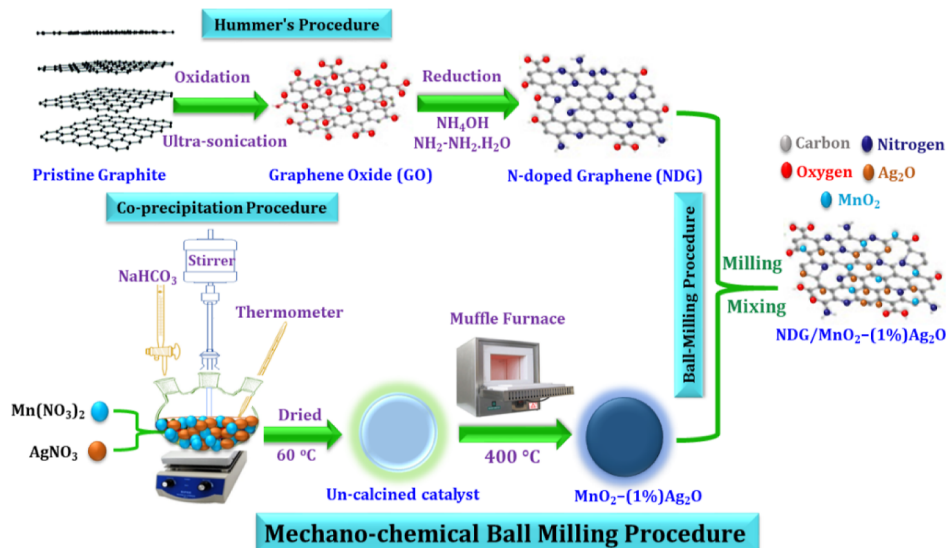
metal NPs (e.g., Cu, Ni, V, Cr, Mo, Fe, Re, and Zr) for the transformation of alcohols to carbonyls.[7,8] Moreover, numerous reported methods stated that the effectiveness of the metal-based catalysts for alcohol oxidation was greatly enhanced after compositing with other metal NPs, presumably because of the synergistic effects between them.[9]

Indeed, metallic NPs are often unstable and easily agglomerate owing to massive surface energy, which consequently reduces their reactivity and stability.[10] Hence, to minimize these disadvantages, metal NPs are immobilized on a suitable dopant or supporting material that has a higher surface area and inhibits the metal NPs from agglomeration.[11] For example, Li et al., have recently reported the preparation of high-performance single-atom catalysts (SACs) using 2D transition-metal dichalcogenides as support.[12] For this purpose, iron atoms were atomically dispersed over defect-containing MoS$_2$ nano-sheets using a reduction approach. The as-prepared iron-based single-atom nanocatalyst has exhibited excellent catalytic activity (1 atm O$_2$ @ 120 °C) toward the selective oxidation of benzyl alcohol to benzaldehyde (∼99% selectivity and ∼100% conversion). Among the different dopants and catalyst supports studied, carbonaceous nanomaterials, particularly graphene derivatives, including GRO, H-RG, and N-DG, have attracted a lot of interest due to their tremendous potential in several applications, like catalysis, supercapacitors, drug delivery, electronics, lithium batteries, sensors, hydrogen storage, and fuel cells.[13] This is owing to the unique physical, chemical, magnetic, electronic, and optical properties of their structure integrity and massive surface area.[14] In their study, Yin et al. have utilized phosphoric acid and N-containing peanut shells (biomass waste) to introduce phosphorus (P) into the carbon skeleton to achieve P-doped porous carbon materials with inherent N functionality.[15] The resulting N-containing, porous carbon materials showed remarkable catalytic activity toward the aerobic oxidation of benzyl alcohol with almost 99% selectivity. Apart from these, several other studies have been reported on the use of heteroatom-doped, supported catalysts for the oxidation of alcohols.[16]

Nitrogen functionality has been used to enhance the structural and electrical properties of graphene, and N-doping assists the electron transfer on the substrate-supported metal

NPs interface to promote the catalyst efficacy and forms numerous structural defects as anchoring sites to improve the dispersing of metal NPs.[17] Moreover, the additional nitrogen atom on the graphene sheet offers a superb alternate for the uniform distribution of metallic NPs on graphene sheets, as it greatly affects the growth mechanism of NPs, which helps in controlling the size and morphology of the NPs. In addition, they assist in the homogeneous dispersion of NPs.[18] Additionally, the high electronegativity of nitrogen compared to carbon leads to the formation of catalytically active sites, due to which N-doped graphene-based nanocomposites have been employed as catalysts for numerous reactions.[19] In addition to the aggregation of metal NPs, the inevitable restacking and agglomeration of graphene sheets led to a decline in their surface areas, therefore making them undesirable for strong adherence and uniform dispersion of active components.[20] Commonly, the restacking and agglomerating of graphene can be prohibited by doping various metals or metal oxide NPs like Pd, Ru, Ag, ZnO, Co$_3$O$_4$, and CeO$_2$ on the graphene layer.[20−22]

Our research group has developed several metal NP-based catalysts and their graphene nanocomposites and investigated their catalytic properties toward the oxidation of alcohols.[6,23,24] In our previously reported investigation, we reported that Ag$_2$O NPs are highly effective dopants for MnO$_2$, and the catalyst (1% Ag$_2$O)−MnO$_2$ calcined at 400 °C afforded outstanding effectiveness for aerobic oxidation of a wide array of alcohols with the eco-friendly oxidant O$_2$, which was later studied by doping the same with GRO and HRG, and their catalytic aptitude was also explored[24,25] Herein, we prepared novel Ag$_2$O−MnO$_2$/(X %)N-DG nanocomposites via a facile and eco-friendly two-steps method with the coprecipitation procedure followed by the mechanochemical ball-milling procedure, as described in Scheme 1, and explored their efficacy with selective aerial oxidation of BlOH as a substrate model. The mechanochemical ball milling technique assists in the inhibition of agglomeration. Additionally, the effects of reaction factors on the catalytic properties of the prepared catalysts are systematically explored. Furthermore, it is interesting to notice that introducing a different percentage of N-DG into the Ag$_2$O−MnO$_2$ nanocatalyst could dramatically improve the catalytic activity for BlOH oxidation. The synthesized materials are fully

characterized by using suitable microscopic and spectroscopic techniques. The fabricated catalysts are tested for the aerobic oxidation of various arrays of alcohols with full convertibility and selectivity. Interestingly, this is the first report using silver oxide NPs-MnO_2 with N-DG as a codopant for alcohol oxidation, highlighting the influence of N-DG in improving the performance of the catalyst system.

2. MATERIALS AND METHODS

2.1. Preparation of GRO and N-DG. The Hummers oxidation procedure is utilized to synthesize GRO.[26] Then, GRO is reduced by adding hydrazine hydrate and ammonium hydroxide to prepare N-DG, and the full synthetic procedure is mentioned in the Supporting Information.

2.2. Preparation of Ag₂O−MnO₂/(X %)N-DG. In brief, Ag_2O nanoparticles−MnO_2 are synthesized by a one-step coprecipitation route in which the stoichiometric concentrations of $Mn(NO_3)_2$ and $AgNO_3$ solutions were mixed and vigorously stirred at 98 °C. After that, the dilute solution of $NaHCO_3$ (0.50 M) is added dropwise into the above mixture solution until it gives a pH value of 9.5; thereafter, the addition of $NaHCO_3$ is stopped, and the resulting solution is continuously stirred for 4 h at identical temperature. Then, the heating is stopped, and the stirring is continued overnight at R.T. The solid powder is filtered using centrifugation and washed many times with distilled water, and then the powder is kept in the oven at 60 °C overnight for drying. The obtained products are calcined at 400 °C in a muffle furnace, and Ag_2O nanoparticles−MnO_2 are obtained. Thereafter, the presynthesized N-DG is dried at 60 °C, followed by grounding in a planetary ball mill. The different wt % of N-DG are mixed with MnO_2−(1% Ag_2O) in a planetary ball milling to obtain MnO_2−(1% Ag_2O)-doped (X %) N-DG nanocomposites, i.e., (X %)N-DG/MnO_2−(1% Ag_2O). The specifics of the planetary ball-milling process are mentioned in the Supporting Information

2.3. Material Characterization and Catalytic Assessment Studies. The details related to the characterization techniques and procedure for the aerial alkali-free oxidation of alcohols have been summarized in Supporting Information

3. RESULTS AND DISCUSSION

3.1. Characterization of Prepared Catalysts. The crystal morphology of synthesized materials is studied via X-ray diffraction (XRD) analysis. Figure 1 displays X-ray diffractograms of pristine graphite, GRO, N-DG, MnO_2−(1% Ag_2O),
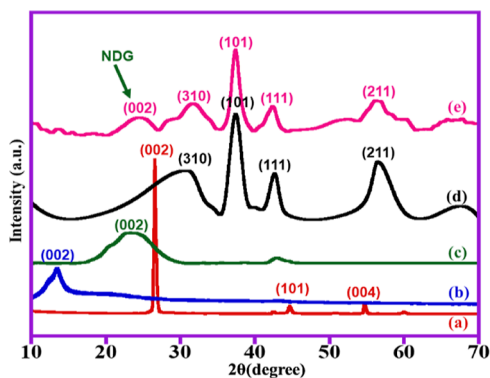

Figure 1. XRD patterns of (a) pure graphite, (b) GRO, (C) N-DG, (d) MnO_2−(1% Ag_2O) catalyst, and (e) (5%)N-DG/MnO_2−(1% Ag_2O) nanocomposite.

and (5%)N-DG/MnO_2−(1% Ag_2O). The XRD pattern of graphite displays a strong (0 0 2) peak located at $2\theta = 26.5°$ for a d-distance of 3.43 Å.[27] However, GRO shows a wide characteristic peak at $2\theta = 11.8°$, ascribed to the (0 0 2) crystal planes and related to a distance d of 6.44 Å. The absence of a graphite peak and the appearance of a novel reflection at approximately 11.8° implies that the total oxidation of graphite to GRO.[28] This shift in 2θ is attributed to the increase in interlayer separation from 3.43 to 6.44 Å for graphite and GRO, respectively, which confirms that the stacked graphite sheets are effectively separated and the presence of surface O-possessing functional groups between the graphene sheets after the oxidation process.[29] XRD diffractogram of pristine N-DG shows a broad peak at $2\theta = 24.6°$ with a (0 0 2) crystal plane, which is a feature band of N-DG, and the absence of the GRO peak at $2\theta = 11.8°$, confirming the successful doping of N atoms into the graphene sheets.[28] XRD pattern for undoped catalyst MnO_2−(1% Ag_2O) (without N-DG) is in accordance with the pyrolusite MnO_2 (JCPDS no. 24-0735).[8] For the (5%)N-DG/MnO_2−(1% Ag_2O) diffractogram, all diffraction peaks are indexed to the well-crystallized pyrolusite MnO_2 structure (JCPDS no. 24-0735) and the fingerprint band of N-DG situated at 24.6°. The average crystallite size of the MnO_2−(1% Ag_2O) in the (5%)N-DG/MnO_2−(1% Ag_2O) nanocomposite is calculated using the Debye−Scherrer formula and is found to be 4.57 ± 1.36 nm, which is smaller than that of MnO_2−(1% Ag_2O), i.e., before milling, which is found to be 11.10 nm.

Thermogravimetric analysis (TGA) is conducted to measure the thermal properties of the synthesized materials from R.T. to 800 °C under a N_2 atmosphere. Figure 2 shows the comparison
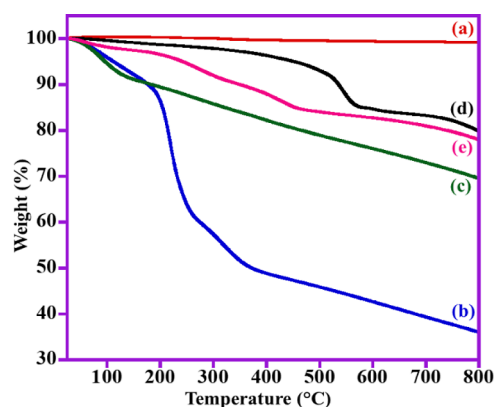

Figure 2. TGA thermograms of (a) pure graphite, (b) GRO, (c) N-DG, (d) MnO_2−(1% Ag_2O) catalyst, and (e) (5%)N-DG/MnO_2−(1% Ag_2O) nanocomposite.

between the thermal properties of the synthesized nanocomposite [i.e., (5%)N-DG/MnO_2−(1% Ag_2O)] and the thermal behaviors of its precursors like graphite, GRO, N-DG, and MnO_2−(1% Ag_2O). Pristine graphite is highly thermally stable and shows a full weight loss of ~1% over a broad range of temperatures (R.T. −800 °C). In contrast, the stability of GRO is much lower than that of pristine graphite. This could be presumably due to the existence of numerous surface oxygen-bearing groups on GRO sheets.[30] TGA curve of GRO shows ~5% weight loss at a temperature of 100 °C, which distinctly might be due to the evaporation of moisture and physisorbed H_2O held on the surface of GRO. The second mass loss of approximately 45% at 200−385 °C could be related to the pyrolysis of oxygenic-carrying groups. Finally, the third weight

loss (~10%) occurred between 385 and 800 °C due to the thermal degradation of the carbon skeleton.[31] Nevertheless, the TGA graph of N-DG exhibits a total mass loss of 28%, ascribed to the reduction of O-containing groups on the graphene surface.

Besides, the (5%)N-DG/MnO$_2$−(1% Ag$_2$O) thermogram exhibited an entire weight loss of ~20% compared to the 18% weight loss exhibited by the MnO$_2$−(1% Ag$_2$O) catalyst over the identical temperature range, suggesting that the doping of the N-DG in the MnO$_2$−(1% Ag$_2$O) catalyst, i.e., the (5%)N-DG/MnO$_2$−(1% Ag$_2$O), slightly reduces its thermal stability.

The FTIR spectrum of the (5%)N-DG/MnO$_2$−(1% Ag$_2$O) catalyst is illustrated in Figure 3, and the FTIR results of N-DG
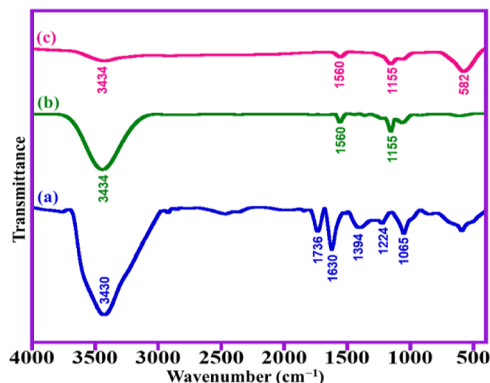
Figure 3. Fourier-transform infrared spectroscopy results of (a) GRO, (b) N-DG, and (c) (5%)N-DG/MnO$_2$−(1% Ag$_2$O) nanocomposite.

and GRO are also shown for comparison. For the GRO, the broad range band at around 3430 cm^{-1} is related to (O−H) stretching vibrations attributed to the existence of oxygen-bearing functionalities. The sharp peak centered at 1736 cm^{-1} is assigned to C=O stretching modes of carboxylic groups, and the peak situated at 1630 cm^{-1} belongs to the carbon skeletal vibrations from nonoxidized graphitic domains.[18] Additionally, the other peaks located at 1065, 1224, and 1394 cm^{-1} are correlated to the vibrations of C−O, C−O−C, and C−OH, respectively.[32] The fingerprint peaks of oxygenated functionalities are distinctly weakened and/or vanished in the spectra of pristine N-DG and (5%)N-DG/MnO$_2$−(1% Ag$_2$O) nanocomposite, confirming that GRO has been reduced efficiently to N-DG. For the N-DG spectrum, some characteristic peaks are detected at 3434 and 1560 cm^{-1}, belonging to stretching modes of N−H, and the peak at ~1155 cm^{-1}, assigned to vibrations of C−N,[33] and other peaks belonging to oxygenic groups, disappeared, as expected. Nonetheless, comparing the GRO spectrum with pure N-DG and (5%)N-DG/MnO$_2$−(1% Ag$_2$O) nanocomposite obviously shows the efficacious reduction of most oxygenated functionalities. As predicted, the spectra of (5%)N-DG/MnO$_2$−(1% Ag$_2$O) nanocomposite show a wide band at 3434 and 1560 cm^{-1} assigned to vibrations of N−H and the absorption peak centered at 1155 cm^{-1} associated with the vibrations of C−N. Finally, the strong peak located at 582 cm^{-1} is assigned to the vibration modes of Mn−O.[34]

Raman analysis is an important characterization technique to estimate the quality of graphene and its derivatives.[35] Figure 4 demonstrates the Raman spectra of GRO, N-DG, and the (5%)N-DG/MnO$_2$−(1% Ag$_2$O) nanocomposite. As shown in Figure 4a, the GRO spectrum illustrates two distinguished bands: the G-band at around 1604 cm^{-1} attributed to the E$_{2g}$-
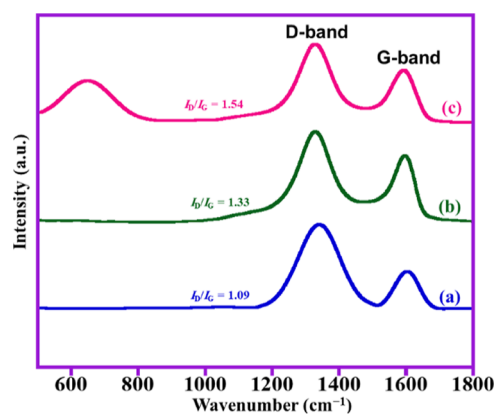

Figure 4. Raman spectra of (a) GRO, (b) N-DG, and (c) (5%)N-DG/MnO$_2$−(1% Ag$_2$O) nanocomposite.

phonon of sp^2 hybrid carbon atoms and the D-band situated at ~1335 cm^{-1} associated with a disordered graphene lattice of A$_{1g}$ symmetry. The G-band is commonly related to the well-order structure of stretching vibrations of the C−C bond, while the D-band is usually generated from the disorder structure, which might be owing to the presence of defects.[36] The defective degree of graphene is usually calculated by the (I_D/I_G) ratio.[35] For the spectra of N-DG and (5%)N-DG/MnO$_2$−(1% Ag$_2$O), the G-band appears at 1595 and 1598 cm^{-1} and the D-band at 1328 and 1328 cm^{-1}, respectively. Notably, the G-band in the N-DG spectra is red-shifted to a low wavenumber due to the oxygen atom being replaced by a nitrogen atom through N doping, which consequently forms pyridinic, pyrrolic, and N-graphitic atoms instead of sp^2-hybridized carbon atoms.[37] The D-band in the GRO spectra has been widened and can be ascribed to the presence of oxygenic functionalities through an oxidation method that disrupts the sp^2 structure. The increment in the number of defects (I_D/I_G) from 1.09 (GRO) to 1.33 (N-DG) indicates that the doping of heterogeneous N-atoms into the graphene nanolayers. Finally, the higher number of defects (I_D/I_G) for (5%)N-DG/MnO$_2$−(1% Ag$_2$O) (1.54), compared with pure N-DG, suggests an increase of defects attributed to N-doping. Besides, the Raman spectrum of the (5%)N-DG/MnO$_2$−(1% Ag$_2$O) nanocomposite displayed a characteristic band located at 644 cm^{-1}. The existence of this band might be ascribed to the symmetric lattice vibrations of Mn−O, implying the presence of MnO$_2$ in the synthesized (5%) N-DG/MnO$_2$−(1% Ag$_2$O) nanocomposite.[38] Fortunately, the obtained Raman results are in full accordance with the XRD and FTIR results.

The morphology of the sample is examined using field emission scanning electron microscopy (FE-SEM). The micrographs of the (5%)N-DG/MnO$_2$−(1% Ag$_2$O) nanocomposite are displayed in Figure 5. From the image Figure 5a, it can be assumed that the N-DG are block-like structures and are immersed inside a pool of MnO$_2$−(1% Ag$_2$O) nanoparticles, which are cubic-shaped, which is evident from the image (Figure 5b). In order to compare the variations in surface area owing to the inclusion of N-DG in the catalyst protocol and to understand the relation between the surface areas and the effectiveness of the prepared materials for alcohol oxidation, the BET surface area analyses of the fabricated materials are measured. Table 1 illustrates that the surface area of pure MnO$_2$−(1% Ag$_2$O) (without N-DG) is about 84 m^2/g. As expected, after incorporating the catalytic system with graphene dopants including N-DG, GRO, and H-RG, the surface areas are
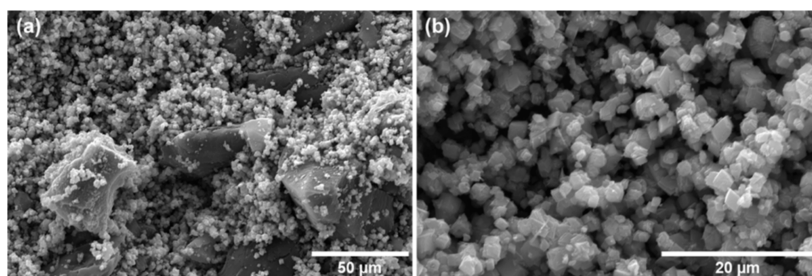
Figure 5. FE-SEM images of the (5%)N-DG/MnO$_2$−(1% Ag$_2$O) nanocomposite at different magnifications [(a) 50 and (b) 20 μm].

Table 1. Oxidation of BlOH Over the Prepared Catalysts with Different Graphene Dopants[a]

sl. no.	catalyst	surface area (m^2/g)	conv. (%)	select. (%)	specific activity (mmol/h/g)
1	MnO$_2$	39	39.6	>99.9	6.33
2	MnO$_2$−(1% Ag$_2$O)	84	62.2	>99.9	9.95
3	(5%)N-DG/MnO$_2$−(1% Ag$_2$O)	163	100.0	>99.9	16.00
4	(5%)GRO/MnO$_2$−(1% Ag$_2$O)	159	95.6	>99.9	15.29
5	(5%)H-RG/MnO$_2$−(1% Ag$_2$O)	149	89.4	>99.9	14.31

[a]Experimental conditions: BlOH (2 mmol), toluene (15 mL), an O$_2$ rate of 20 mL/min, a catalyst dose of 300 mg, an operating temperature of 100 °C, and a period of 25 min.

markedly raised to 164, 159, and 149 m^2/g, respectively. It is noteworthy that the catalytic results of the as-made samples relate well to the surface area. Noticeably, the catalytic aptitude after doping MnO$_2$−(1% Ag$_2$O) with N-DG, GRO, and H-RG, i.e., (5%)N-DG/MnO$_2$−(1% Ag$_2$O), (5%)GRO/MnO$_2$−(1% Ag$_2$O), and (5%)H-RG/MnO$_2$−(1% Ag$_2$O), respectively, was also considerably enhanced. Hence, it could be stated that the compositing graphene dopants (i.e., N-DG, GRO, or H-RG) to the catalyst protocol had a positive influence on surface area, which necessarily leads to an increase in the efficacy of the catalytic system. Ultimately, the (5%)N-DG/MnO$_2$−(1% Ag$_2$O) nanocomposite has the maximum surface area and affords the highest conversion of BlOH compared with other catalysts, whereas other synthesized catalysts possess lower catalytic performance and surface area.

3.2. Catalytic Assessment Tests. The major target of the current report is alcohol oxidation with both high convertibility and selectivity, employing dioxygen as an ecofriendly oxidizing agent with no use of alkalis or surfactants. To realize this aim, we have utilized N-DG as a codopant for the Ag$_2$O NP-doped MnO$_2$ catalyst in the aerial selective oxidation of BlOH as the probe molecule to BlCHO under alkali-free circumstances, as described in Scheme 2. It has been observed that this oxidation transformation has been markedly affected by different reaction factors, including various percentages of N-DG, various graphene dopants, reaction period, catalyst concentration, and operating temperature, as demonstrated in Figures 6−9.

3.2.1. Impact of Different Graphene Dopants. Subsequently, we have compared the catalytic aptitude of MnO$_2$−(1% Ag$_2$O) catalysts doped with various graphene dopants (GRO, H-RG, and N-DG) for selective aerial oxidation of BlOH to realize the effect of graphene on the activity of the catalyst system, and the attained data are collected in Table 1. Initially, we examined a pure MnO$_2$ sample for this oxidation process under the aforementioned conditions, and a 39.58% conversion in 25 min was detected, while after doing it with 1% of Ag$_2$O, i.e., MnO$_2$−(1% Ag$_2$O), the BlOH conversion significantly increased and yielded 62.2% alcohol conversion at the same conditions. Nevertheless, further modifications have been carried out by doping N-DG as a codopant to the MnO$_2$−(1%

Scheme 2. Scheme Depiction of BlOH Dehydrogenation in the Presence of O$_2$ Over the (X %)N-DG/MnO$_2$−(1% Ag$_2$O) Nanocomposite
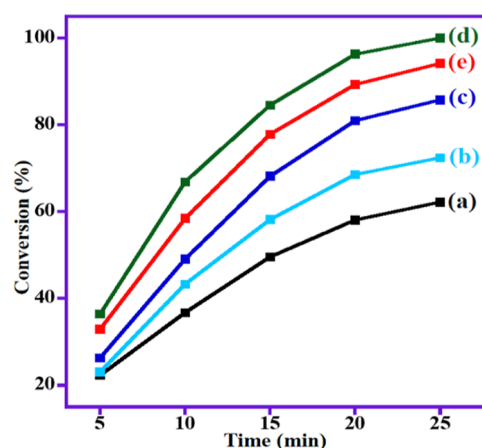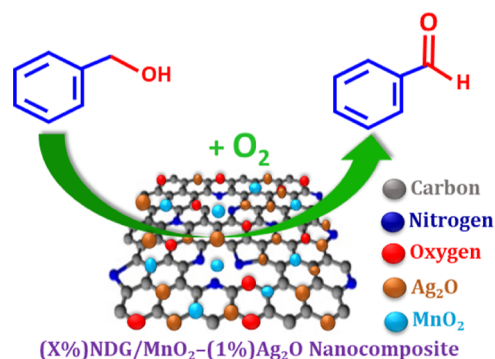

Figure 6. Graphical presentation of BlOH oxidation over (a) MnO$_2$−(1% Ag$_2$O), (b) (1%)N-DG/MnO$_2$−(1% Ag$_2$O), (c) (3%)N-DG/MnO$_2$−(1% Ag$_2$O), (d) (5%)N-DG/MnO$_2$−(1% Ag$_2$O), and (e) (7%)N-DG/MnO$_2$−(1% Ag$_2$O) nanocomposites.

Ag$_2$O) nanocatalyst, i.e., (5%)N-DG/MnO$_2$−(1% Ag$_2$O) has higher performance than the nanocomposites codoped with GRO and H-RG, i.e., (5%)GRO/MnO$_2$−(1% Ag$_2$O) and
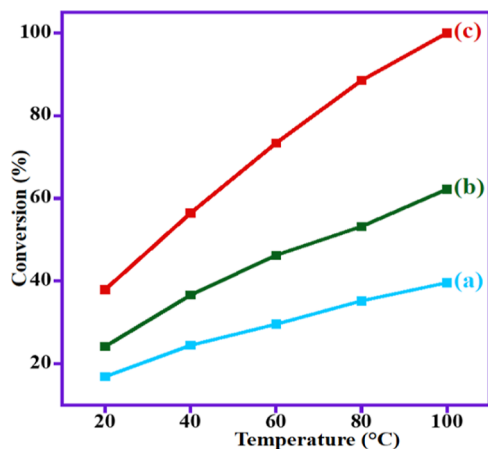
Figure 7. Effect of operating temperature on BlOH oxidation over (a) MnO_2, (b) $MnO_2-(1\% Ag_2O)$, and (c) $(5\%)N-DG/MnO_2-(1\% Ag_2O)$.
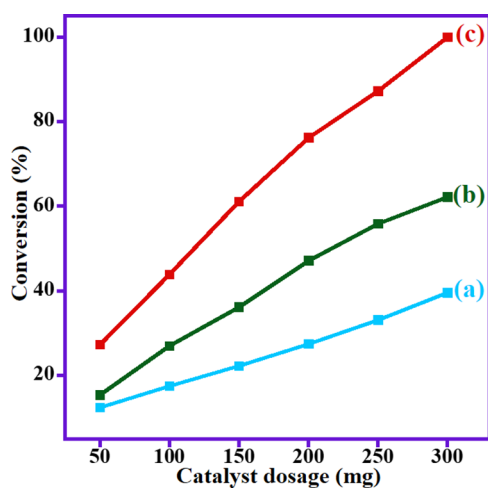

Figure 8. Effect of changing catalyst dosage on BlOH oxidation catalyzed by (a) MnO_2, (b) $MnO_2-(1\% Ag_2O)$, and (c) $(5\%)N-DG/MnO_2-(1\% Ag_2O)$.

$(5\%)H-RG/MnO_2-(1\% Ag_2O)$, respectively. The $(5\%)N-DG/MnO_2-(1\% Ag_2O)$ catalyst exhibits the best performance and yields 100% transformation of BlOH with a premium specific activity of 16.0 mmol/h/g within short intervals (25 min). The GRO-based nanocomposite, i.e., $(5\%)GRO/MnO_2-(1\% Ag_2O)$ gave a 95.6% conversion of BlOH in addition to 15.29 mmol/h/g specific activity. The enhanced activity after the introduction of GRO in the catalyst system might be ascribed to the existence of oxygenic-possessing groups in GRO assisting the oxidation of alcohol.[39] It is noteworthy that after inclusion of H-RG in $MnO_2-(1\% Ag_2O)$ nanocatalyst, the $(5\%)H-RG/MnO_2-(1\% Ag_2O)$ afforded higher efficiency relative to $MnO_2-(1\% Ag_2O)$ without codopant (H-RG), presumably owing to the increase adsorption between π-electrons on the H-RG surface and π-electrons on the aromatic substrates (BlOH) through the $\pi-\pi$ interaction near catalytic active sites of the catalyst $[MnO_2-(1\% Ag_2O)]$.[24] The improved activity of the N-DG-based catalyst could be ascribed to the presence of the nitrogen atoms on the N-DG surface; moreover, the extra electronic density compared to the carbon atoms is because of the presence of the nitrogen atoms.[22] Ultimately, the existence of N-DG could be responsible for more defects in the crystalline
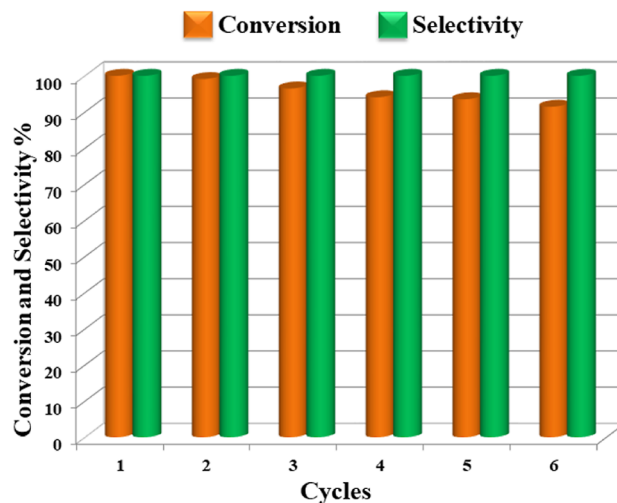
Figure 9. Recyclability results of the $(5\%)N-DG/MnO_2-(1\% Ag_2O)$ catalyst for selective oxidation of BlOH. Experimental conditions: BlOH (2.0 mmol), flow rate of O_2 (20 mL/min), toluene (15 mL), catalyst dose (0.30 g), operating temperature (100 °C), and time (25 min).

catalysts [i.e., $MnO_2-(1\% Ag_2O)$], which improves the efficiency of the catalytic protocol.

The same reaction is carried out under solvent-free conditions while maintaining the other parameters identical, and a 34% conversion product is obtained, while the selectivity was >99%.

3.2.2. Effect of wt Percentage of N-DG. In most cases, the efficacy of the oxidation catalyst can be fine-tuned after utilizing carbonaceous materials, particularly graphene as a catalyst support or a dopant.[40−42] In our previous study, we reported that the Ag_2O nanoparticles are superb dopants for the MnO_2 nanocatalyst, and $MnO_2-(1\% Ag_2O)$ catalyst at 400 °C annealing temperature exhibited outstanding catalytic aptitude for aerial selective oxidation of alcohols, with dioxygen serving as an eco-friendly oxidizing agent.[8] Subsequently, herein, the $MnO_2-(1\% Ag_2O)$ catalyst is selected and further modified by doping it with different weight percentages of N-DG to further enhance its activity. However, the initial investigations were conducted to find out the appropriate wt % of N-DG in the prepared nanocomposite. Initially, the effectiveness of pristine N-DG has been examined toward aerobic BlOH oxidation, and it was found that the N-DG exhibits very low performance and can be neglected.

The catalytic properties of various $(X \%)N-DG/MnO_2-(1\% Ag_2O)$ nanocomposites, in which the weight percentage of N-DG is varied from 1 to 7 wt %, and their activities are examined for oxidation of BlOH, and the catalytic results are compiled in Table 2 and Figure 6. As displayed in Table 2 and Figure 6, the $[MnO_2-(1\% Ag_2O)]$ catalyst without N-DG gave a 62.2% BlOH conversion in 25 min. Nevertheless, after doping the synthesized catalyst with 1 and 3 wt % N-DG, i.e., $(1\%)N-DG/MnO_2-(1\% Ag_2O)$ and $(3\%)N-DG/MnO_2-(1\% Ag_2O)$, the nanocomposites afford BlOH conversion of 72.4% and 85.8%, respectively, at the same practical conditions. Further raising the weight % of N-DG in the nanocomposite to 5%, i.e., $(5\%)N-DG/MnO_2-(1\% Ag_2O)$, the performance considerably increases and yields a 100% conversion in 25 min and a premium specific activity of 16.0 mmol/h/g. When the weight % of N-DG further increases to 7%, the efficacy of the nanocomposite slightly declines to 94.15%, possibly attributed to the blocking

Table 2. Catalytic Oxidation of BlOH to BlCHO Over the Several Synthesized Catalysts[a]

sl. no.	catalyst	conv. (%)	select. (%)	specific activity (mmol/h/g)
1	N-DG	3.2	>99.9	0.51
2	$MnO_2-(1\% Ag_2O)$	62.2	>99.9	9.95
3	$(1\%)N\text{-}DG/MnO_2-(1\% Ag_2O)$	72.4	>99.9	11.58
4	$(3\%)N\text{-}DG/MnO_2-(1\% Ag_2O)$	85.8	>99.9	13.72
5	$(5\%)N\text{-}DG/MnO_2-(1\% Ag_2O)$	100.0	>99.9	16.0
6	$(5\%)N\text{-}DG/MnO_2-(1\% Ag_2O)$ [S]	47	>99.9	6.89
7	$(5\%)N\text{-}DG/MnO_2-(1\% Ag_2O)$ [solvent-free]	34	>99.9	5.44
7	$(7\%)N\text{-}DG/MnO_2-(1\% Ag_2O)$	94.2	>99.9	15.06

[a]Experimental conditions: BlOH (2 mmol), toluene (15 mL), O_2 rate of 20 mL/min, catalyst dose of 300 mg, operating temperature of 100 °C, and a period of 25 min.

effect of N-DG that may block the catalytic active sites of the catalyst due to the high weight % of N-DG. In addition, the BlCHO selectivity remains constant during all oxidation reactions (>99.9%). As a result, it can be stated that the N-DG had a pivotal impact in promoting the efficacy of the present catalytic methodology for this oxidation process. Eventually, the results disclose that $(5\%)N\text{-}DG/MnO_2-(1\% Ag_2O)$ is the preferable catalyst among all other fabricated catalysts and will be utilized in further optimization studies.

In addition to the role played by the presence of N-DG in the catalyst system, the role of ball milling in the enhancement of the efficiency of the catalyst system was evaluated. The superior catalytic activity among the as-prepared catalysts, i.e., $(5\%)N\text{-}DG/MnO_2-(1\% Ag_2O)$[S] (Figure S1), was prepared by mixing the components of the composite, i.e., N-DG and $MnO_2-(1\% Ag_2O)$ using a spatula, and the nanocomposite obtained was employed for the catalytic oxidation of BlOH, which gave a 47% conversion product, unlike the 100% conversion obtained when the $(5\%)N\text{-}DG/MnO_2-(1\% Ag_2O)$ prepared by ball milling was used. Hence, it can be concluded that the ball milling procedure employed plays a significant role in the catalytic performance of the nanocomposite, just like previous reports wherein the ball milling of several metal oxides had a favorable effect on their properties.[43] In addition to the comparative catalytic performance study, the morphology of the catalyst prepared by simple mixing using a spatula, i.e., $(5\%)N\text{-}DG/MnO_2-(1\% Ag_2O)$[S] was evaluated using SEM analysis, and the micrograph obtained was compared to the catalyst obtained by ball milling (cf. Figure S1). It can be observed that the N-DG component of the catalyst is noninteractive with the $MnO_2-(1\% Ag_2O)$, while in the microgram obtained for the sample prepared using ball milling, it can be clearly observed that there is intense interaction between the two components, most probably enforced due to the procedure employed, which in turn has an assenting influence on the catalytic performance.

3.2.3. Impact of the Operating Temperature. Ordinarily, the operating temperature plays a vital role in the catalyst system and has a pronounced impact on the efficacy of catalysts. Accordingly, the impact of temperature on the BlOH oxidation is also assessed by carrying out the reactions in R.T., 40, 60, 80, and 100 °C with the prepared catalysts [i.e., MnO_2, $MnO_2-(1\% Ag_2O)$ and $(5\%)N\text{-}DG/MnO_2-(1\% Ag_2O)$] while keeping other reaction variables constant. According to Figure 7, the operating temperature has a positive influence on the performance of all of the catalysts applied in the current report. Meantime, outstanding selectivity toward BlCHO (typically >99.9%) is accomplished for all catalysts. Among all of the catalysts, the $(5\%)N\text{-}DG/MnO_2-(1\% Ag_2O)$ catalyst yielded

the maximum catalytic performance. A low alcohol conversion of 37.9% is detected when the experiment is carried out at a lower operation temperature (i.e., R.T.). As it is predictable, with raising the temperature to 100 °C, an entire conversion of BlOH is accomplished under other identical experimental circumstances. Therefore, the optimal reaction temperature for this study is 100 °C.

3.2.4. Impact of Catalyst Dose. Furthermore, optimization studies of the catalyst dose are performed by varying the catalyst quantity from 50.0 to 300 mg. Subsequently, the impact of the amount of the as-made catalysts [i.e., MnO_2, $MnO_2-(1\% Ag_2O)$, and $(5\%)N\text{-}DG/MnO_2-(1\% Ag_2O)$] is tested while preserving other experimental factors, and the achieved observations are plotted in Figure 8. When the oxidation process is conducted in the absence of the prepared catalyst, we have found that no product BlCHO is detected, suggesting that the catalyst is indispensable for the current oxidation reaction. Figure 8 distinctly shows that the alcohol conversion increased linearly with the rising catalyst quantity from 50.0 to 300 mg. While the selectivity of BlCHO is unaltered through all oxidation tests (<99.9%). Distinctly, the results verified that the $(5\%)N\text{-}DG/MnO_2-(1\% Ag_2O)$ catalyst showed maximal effectiveness compared with other catalysts, and the conversion rose greatly from 27.25% to 100% as the amounts of catalyst rose from 50.0 to 300 mg in just 25 min, indicating that the catalysis is being carried out outside the diffusion limitation.

At optimized experimental conditions, a blank test is conducted utilizing $(5\%)N\text{-}DG/MnO_2-(1\% Ag_2O)$ without using any substrate (BlOH) or solvent (toluene) to emphasize that there is no function of toluene in the BlOH oxidation to BlCHO. As expected, the oxidative yield (BlCHO) is not detected, deducing that the BH is formed only as a result of the selective oxidation of BlOH and not generated from the oxidation of toluene under the aforementioned conditions. Moreover, to understand the significance of the oxidant (O_2 molecule) for the present oxidation process, the experiment is carried out using $(5\%)N\text{-}DG/MnO_2-(1\% Ag_2O)$ utilizing atmospheric air instead of molecular O_2, and it is observed that the as-obtained catalyst shows conversion of only 23.8% compared to the 100% conversion for a reaction carried out using O_2, which suggests the pivotal role of molecular O_2.

3.3. Catalyst Recyclability Evaluation. Catalyst recyclability is an extremely important aspect from both environmental and industrial viewpoints. Therefore, the reutilization of $(5\%)N\text{-}DG/MnO_2-(1\% Ag_2O)$ nanocomposite for aerobic oxidation of BlOH with an O_2 molecule is tested under optimum circumstances. After each recycling reaction, the used sample is recovered by centrifugation, then filtration, washed thoroughly with toluene for cleaning the surface of the catalyst, followed by

Table 3. Comparative Data of the Catalytic Oxidation of BlOH Over Several Catalytic Systems with Graphene

catalyst	time (h)	T (°C)	conv. (%)	select. (%)	sp. Activity (mmol/h/g)	ref
(5%)N-DG/MnO$_2$−(1% Ag$_2$O)	0.42	100	100	<99.9	16.0	this study
(5%)H-RG/MnO$_2$−(1% Ag$_2$O)	0.42	100	100	<99.9	15.29	24
(5%)GRO/MnO$_2$−(1% Ag$_2$O)	0.42	100	100	<99.9	14.31	25
Au NPs/N-DG	6	70	67	40	0.4	45
Co NPs/N-DG	8	100	89.5	97.3	4.5	46
Pd NPs/GO	6	110	36	34.1	1.0	47
Cu NPs/rGO	16	80	<99	98.6	8.3	48
4% Ru(CO)/N-DG	24	90	46	<99	6.4	22
Fe$_3$O$_4$−Pt NPs/rGO	3	80	33.6	100	42.0	49
0.3% Sn−W/RGO	3	80	94	94.3	15.7	40
Fe$_3$O$_4$/HPW/GRO	3	70	99	100	16.7	50
MnCoO/RGO	2	140	78	100	12.6	51
MnO$_2$/GRO	3	110	97	100	1.6	41

drying at 100 °C for 4 h to reactivate the catalyst, to be reused for the next recycling run.

The results indicate that the (5%)N-DG/MnO$_2$−(1% Ag$_2$O) catalyst manifested superior durability and can be reused for 6 runs without notable loss in its efficacy. As seen in Figure 9, the BlOH conversion is slightly reduced from 100 to 91.4% after 6 cycles, and the selectivity toward BlCHO stays constant (typically >99.9%) through these recycling runs. The trivial decline in activity is possibly attributed to the small mass loss of the prepared sample over the filtration step.[44]

Accordingly, the attained data revealed that the (5%)N-DG/MnO$_2$−(1% Ag$_2$O) catalyst has excellent durability and recyclability, which is potentially beneficial for chemical industries.
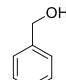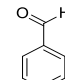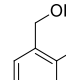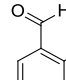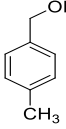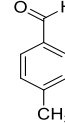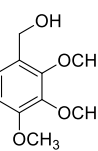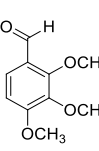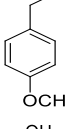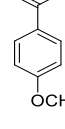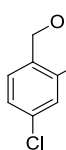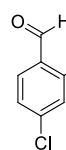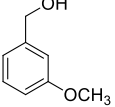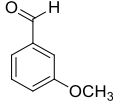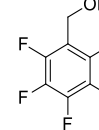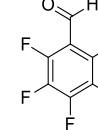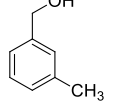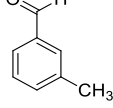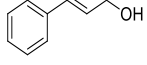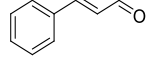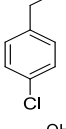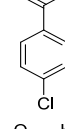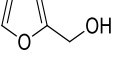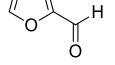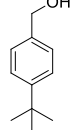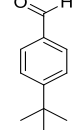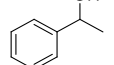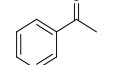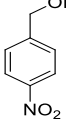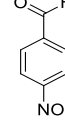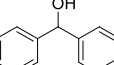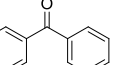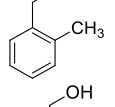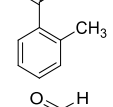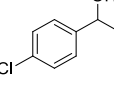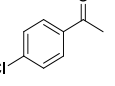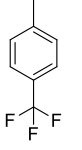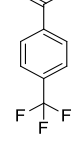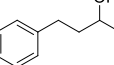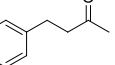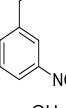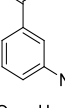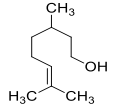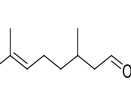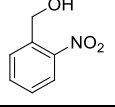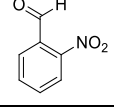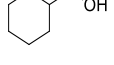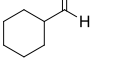
The catalytic efficacy for base-free selective aerial oxidation of BlOH to BlCHO over the (5%)N-DG/MnO$_2$−(1% Ag$_2$O) catalyst in the current investigation and previously published graphene-based catalysts is compared in Table 3. Compared to the listed graphene-based catalysts compiled in Table 3, the (5%)N-DG/MnO$_2$−(1% Ag$_2$O) catalyst in this study showed the highest conversion, specific activity, and selectivity, as well as the shortest reaction time for this transformation. The (5%)N-DG/MnO$_2$−(1% Ag$_2$O) nanocomposite shows 100% BlOH transformation and >99.9% BlCHO selectivity within quite a short time of 25 min with superb specific activity (16.0 mmol/h/g). The data distinctly verified that other catalytic systems containing graphene showed lower conversion and specific activity within an extremely long time with respect to the as-made catalyst. This is presumably attributed to the increment in surface defects, distortions, and vacancies in the N-DG nanosheets, which had an explicit impact on promoting the catalytic activity. In this regard, Xie et al.[45] reported selective oxidation of BlOH catalyzed by Au NPs/N-DG nanocomposite with H$_2$O$_2$ as a green oxidant with 67% alcohol conversion, 40% selectivity toward BlCHO, and 0.40 mmol/h/g specific activity after 6 h. Besides, Ramirez-Barria et al.[22] have fabricated Ru NPs immobilized on N-DG (4% Ru(CO)/N-DG) and used them for selective aerobic oxidation of BlOH with O$_2$ as an ecologically friendly oxidant. The 4% Ru(CO)/N-DG catalyst gave just 46% BlOH conversion and <99% selectivity to BlCHO, with a lower specific activity of 6.4 mmol/h/g within an extremely long operation period (24 h) compared with our catalyst.

3.4. Aerial Selective Oxidation of Other Alcohols by (5%)N-DG/MnO$_2$−(1% Ag$_2$O). Encouraged by the aforementioned superior results, the optimal circumstances are applied to the aerial oxidation of structurally diverse alcohols, including primary, benzylic, heterocyclic, aliphatic, secondary, and allylic alcohols, in the presence of (5%)N-DG/MnO$_2$−(1% Ag$_2$O) nanocomposite as the catalyst employing dioxygen as an environmentally friendly oxidant (Table 4). The results obtained show that all primary aromatic alcohol derivatives are oxidized to desired products in short intervals at optimal conditions without over-oxidation product such as benzoic acid. It is interesting to note that superb selectivities to corresponding carbonyls (aldehydes or ketones) (typically >99.9%) are achieved for most of the alcohols employed in this report, and no undesirable products are observed. The catalytic efficacy is significantly dependent on the electronic properties of groups linked to the aromatic alcohols, relying on their capability to give electrons to the phenyl ring.[52] As predictable, the electron-rich aromatic substrates carrying electron-releasing groups have higher reactivity and show shorter times, whereas the oxidation times for the aromatic substrates with electron-deficient groups are relatively longer.[53] It is noteworthy that aromatic substrates that contain an electron-donating group, such as 4-methoxybenzyl alcohol, are fully transformed to 4-methoxy-benzaldehyde in 35 min. In contrast, 4-trifluoromethylbenzyl alcohol that has an electron-withdrawing substituent needs a relatively longer time of 65 min. Besides, it is observed that the para-substituted benzylic alcohols are fully oxidized within comparatively shorter times comparing with ortho- and meta-positions maybe attributed to the para-position possessing lowest steric hindrance compared with other positions.[54] In this context, the complete oxidation of *para*-nitrobenzyl alcohol takes place in 55 min, while *meta*- and *ortho*-nitrobenzyl alcohols are fully oxidized to respective aldehyde derivatives at comparatively longer times of about 65 and 80 min, respectively, relative to 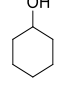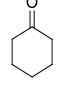para-position. Moreover, steric resistance is also a pivotal parameter that affects the catalytic performances ascribed to the bulky substituents (trimethoxy, trifluoromethyl, dichloro, and pentafluoro) connected to the phenyl ring minimizes the oxidation rate and needs a longer reaction time. This could be owing to the fact that steric resistance hinders the interaction of the alcohol with the catalyst surface, in-turn affecting the oxidation rate of bulky alcohols.[55] Notably, the present catalytic methodology has been found to be efficient for the oxidation of allylic alcohols; for example, cinnamic alcohol is fully transformed to cinnamic aldehyde within 45 min of the reaction. Moreover, a heteroaromatic alcohol such as furfuryl alcohol is selectively transformed to fural in 120 min.

It is important to note that the present catalytic strategy has been found to be efficacious toward selective oxidation of

Table 4. General Applicability of the (5%)N-DG/MnO$_2$−(1% Ag$_2$O) Catalyst in the Selective Base-Free Oxidation of Alcohol Derivatives with O$_2$[a]

Sl.No.	Substrates	Carbonyls	Time (mins)	Conv. (%)/ Select. (%)	Sl.No.	Substrates	Carbonyls	Time (mins)	Conv. (%)/ Select. (%)
1	(benzyl alcohol)	(benzaldehyde)	25	100/ > 99.9	13	(2-chlorobenzyl alcohol)	(2-chlorobenzaldehyde)	65	100/ > 99.9
2	(4-methylbenzyl alcohol)	(4-methylbenzaldehyde)	30	100/ > 99.9	14	(2,3,4-trimethoxybenzyl alcohol)	(2,3,4-trimethoxybenzaldehyde)	70	100/ > 99.9
3	(4-methoxybenzyl alcohol)	(4-methoxybenzaldehyde)	35	100/ > 99.9	15	(2,4-dichlorobenzyl alcohol)	(2,4-dichlorobenzaldehyde)	75	100/ > 99.9
4	(3-methoxybenzyl alcohol)	(3-methoxybenzaldehyde)	45	100/ > 99.9	16	(pentafluorobenzyl alcohol)	(pentafluorobenzaldehyde)	80	100/ > 99.9
5	(3-methylbenzyl alcohol)	(3-methylbenzaldehyde)	40	100/ > 99.9	17	(cinnamyl alcohol)	(cinnamaldehyde)	45	100/ > 99.9
6	(4-chlorobenzyl alcohol)	(4-chlorobenzaldehyde)	45	100/ > 99.9	18	(furfuryl alcohol)	(furfural)	120	100/ > 99.9
7	(4-tert-butylbenzyl alcohol)	(4-tert-butylbenzaldehyde)	50	100/ > 99.9	19	(1-phenylethanol)	(acetophenone)	30	100/ > 99.9
8	(4-nitrobenzyl alcohol)	(4-nitrobenzaldehyde)	55	100/ > 99.9	20	(benzhydrol)	(benzophenone)	40	100/ > 99.9
9	(2-methylbenzyl alcohol)	(2-methylbenzaldehyde)	55	100/ > 99.9	21	(1-(4-chlorophenyl)ethanol)	(4-chloroacetophenone)	45	100/ > 99.9
10	(4-trifluoromethylbenzyl alcohol)	(4-trifluoromethylbenzaldehyde)	65	100/ > 99.9	22	(4-phenyl-2-butanol)	(4-phenyl-2-butanone)	55	100/ > 99.9
11	(3-nitrobenzyl alcohol)	(3-nitrobenzaldehyde)	65	100/ > 99.9	23	(citronellol)	(citronellal)	150	100/ > 99.9
12	(2-nitrobenzyl alcohol)	(2-nitrobenzaldehyde)	80	100/ > 99.9	24	(cyclohexylmethanol)	(cyclohexanecarbaldehyde)	90	100/ > 99.9
					25	(1-heptanol)	(heptanal)	230	100/ > 99.9
					26	(cyclohexanol)	(cyclohexanone)	90	100/ > 99.9
					27	(2-octanol)	(2-octanone)	250	100/ > 99.9

[a]Experimental conditions: alcohol (2.0 mmol), (5%)N-DG/MnO$_2$−(1% Ag$_2$O) catalyst, catalyst dose of 0.30 g, O$_2$ rate of 20 mL/min, toluene (15 mL), and operating temperature of 100 °C.

secondary aromatic alcohols, and complete conversion as well as selectivity toward respective ketone derivatives are achieved.

The total oxidation of styrallyl alcohol to acetophenone occurred in just 30 min, while 1-(4-chlorophenyl)ethanol also

affords 100% conversion but in a longer time of 45 min; this presumably is due to the presence of an electron-withdrawing substituent in the 1-(4-chlorophenyl)ethanol that deactivates the aromatic ring by reducing the electron density.

Indeed, the benzylic substrates are relatively more active than their aliphatic counterparts.[56] The complete oxidation of 1-octanol, citronellol, and cyclohexylmethanol takes place over longer periods time. Likewise, the selective oxidation of secondary aliphatic alcohols shows lower reactivity relative to secondary aromatic alcohols. As estimated, it is necessary to prolong the reaction time, attributed to the fact that the oxidation of aliphatic substrates is more difficult than that of aromatic counterparts. Unsurprisingly, the entire oxidation of styrallyl alcohol happened within 30 min, while the total oxidation of 2-octanol happened in an extremely longer time, i.e., 250 min. Based on that, the efficacy of this catalytic methodology is strongly impacted by two variables: steric hindrance and electronic properties.

3.5. Possible Role of Ag$_2$O and MnO$_2$ in the Oxidation of Alcohol. Typically, during the oxidation of alcohols, gold-based catalysts exhibit higher activity and selectivity than various other noble metal catalysts, including Pt and Pd.[57] However, gold catalysts suffer from various problems, including rapid deactivation and high cost. Although silver-based compounds have long been used for the oxidation of alcohols, they were largely applied for gas-phase reactions.[58] Gradually, silver-based catalysts have also been gaining prominence in liquid-phase oxidation reactions. This information is unsystematic and very scattered on two aspects: catalytic systems and reactions studied.[59] Typically, during the oxidation of alcohols, the basic species is an important factor.[60] Thus, the basic strength of the active sites is crucial, as demonstrated by Sanderson et al. The results revealed that the oxygen in Ag$_2$O has the most negative effective charge, −0.46e, among the transition metal oxides, and that of Cu$_2$O is −0.44.[61] Therefore, the oxygen species of silver oxides are the strongest basic species among other oxides, which exhibit more negative charge.[62] Typically, the acidic sites often promote alcohol dehydration, and the basic sites favor alcohol dehydrogenation.[63] Thus, in this case, possibly, the facets of silver in Ag$_2$O act as ideal multifunctional facets that facilitate the regeneration of oxidative, strong basic oxygen species and weak acidic sites quickly for the catalytic cycles, such as molecular oxygen activation, alcohol chemical adsorption, and the subsequent dehydrogenation. On the other hand, manganese oxides are known to exhibit strong oxidizing properties toward small organic molecules and thus have been used in alcohol oxidation reactions.[64] Besides, they demonstrate excellent proton conductivity and good recyclability due to the synergistic effect between the active metal component and the oxide.

4. CONCLUSIONS

In this study, we have efficiently prepared Ag$_2$O NPs doped MnO$_2$ codoped with N-DG, i.e., (X %)N-DG/MnO$_2$−(1% Ag$_2$O) nanocomposites through a coprecipitation process followed by mechanochemical procedure and applied as an efficacious catalyst for aerobic base-free oxidation of various benzylic, aliphatic, primary, secondary, heterocyclic, and allylic alcohols with O$_2$ as a nature-friendly oxidant under mild conditions. In addition, we have compared the effectiveness of MnO$_2$−(1% Ag$_2$O) doped with various graphene dopants, including N-DG, GRO, and H-RG for this oxidation process to comprehend the graphene role in the catalytic protocol. The results distinctly disclose that the N-DG/MnO$_2$−(1% Ag$_2$O)

has higher performance than the undoped catalysts MnO$_2$−(1% Ag$_2$O), GRO/MnO$_2$−(1% Ag$_2$O), and H-RG/MnO$_2$−(1% Ag$_2$O). The increased effectiveness of the N-DG/MnO$_2$−(1% Ag$_2$O) nanocomposite is possibly due to the existence of N-DG, which influences the interactions between nitrogen atoms on the N-DG surface and MnO$_2$−(1% Ag$_2$O) NPs. The presence of graphene sheets offers several defects and distortions in structure, which led to an increase in the adsorption of aromatic substrates near the active sites, and it can improve the interactions among N-DG surface and acidic substrates, which leads to superb catalytic performances. The (5%)N-DG/MnO$_2$−(1% Ag$_2$O) catalyst exhibits impressive catalytic efficacy (100% conversion and >99.9% selectivity toward BlCHO) for selective alkali-free oxidation of BlOH in quite a short time. Very interestingly, the prepared catalyst presented a premium specific activity (16.0 mmol/h/g) in comparison with other previously reported graphene-based catalysts. Importantly, the oxidation of aromatic substrates is extremely easier than aliphatic counterparts and might be ascribed to the strong interactions (π−π stacking) among aromatic alcohols and graphene layers. (5%)N-DG/MnO$_2$−(1% Ag$_2$O) is stable without notable activity and selectivity decline after six recycling runs. The prime features of this catalytic methodology are (I) facile straightforwardness, (II) readily available precursors, (III) additive-base-free oxidation, (IV) environmentally friendly and low-cost oxidant, (V) inexpensive recoverable catalyst, (VI) mild conditions, (VII) entire convertibility and high selectivity, (VIII) short time of reaction, and (IX) applicability to all types of alcohols.

■ ASSOCIATED CONTENT

Ⓢ **Supporting Information**

The Supporting Information is available free of charge at https://pubs.acs.org/doi/10.1021/acsomega.3c07865.

> Synthesis of GO and NDG, the mechanochemical ball milling procedure of N-DG/MnO$_2$−(1% Ag$_2$O), characterization of synthesized nanocomposites, catalytic activity protocol, and comparison of FE-SEM images of the nanocomposites before and after ball milling. (PDF)

■ AUTHOR INFORMATION

Corresponding Author

Syed Farooq Adil − *Department of Chemistry, College of Science, King Saud University, Riyadh 11451, Saudi Arabia;* ⓞ orcid.org/0000-0002-2768-1235; Phone: +966-11-4670439; Email: sfadil@ksu.edu.sa

Authors

Mohammad Rafe Hatshan − *Department of Chemistry, College of Science, King Saud University, Riyadh 11451, Saudi Arabia*

Mujeeb Khan − *Department of Chemistry, College of Science, King Saud University, Riyadh 11451, Saudi Arabia;* ⓞ orcid.org/0000-0002-4088-6913

Mohamed E. Assal − *Department of Chemistry, College of Science, King Saud University, Riyadh 11451, Saudi Arabia*

Mohammed Rafi Shaik − *Department of Chemistry, College of Science, King Saud University, Riyadh 11451, Saudi Arabia;* ⓞ orcid.org/0000-0003-2937-317X

Mufsir Kuniyil − *Department of Chemistry, College of Science, King Saud University, Riyadh 11451, Saudi Arabia*

Abdulrahman Al-warthan − *Department of Chemistry, College of Science, King Saud University, Riyadh 11451, Saudi Arabia*

Mohammed Rafiq H. Siddiqui − *Department of Chemistry, University of Liverpool, Liverpool L69 7ZD, United Kingdom*

■ REFERENCES

(1) Dai, R.; Eser, B. E.; Guo, Z. Beyond flower-like structure-The synergy within Pd/Ni-Al hydrotalcite for base-free oxidation of benzyl alcohols. *Appl. Catal., A* **2021**, *610*, 117972.

(2) Luo, J.; Peng, F.; Yu, H.; Wang, H. Selective liquid phase oxidation of benzyl alcohol catalyzed by carbon nanotubes. *Chem. Eng. J.* **2012**, *204−206*, 98−106.

(3) Akbari, A.; Amini, M.; Tarassoli, A.; Eftekhari-Sis, B.; Ghasemian, N.; Jabbari, E. Transition metal oxide nanoparticles as efficient catalysts in oxidation reactions. *Nano-Struct. Nano-Objects* **2018**, *14*, 19−48.

(4) Liang, Y.-F.; Jiao, N. Oxygenation via C-H/C-C Bond Activation with Molecular Oxygen. *Acc. Chem. Res.* **2017**, *50* (7), 1640−1653.

(5) Pordel, S.; Rabbani, M.; Rahimi, R.; Heidari-Golafzani, M.; Azad, A. Synthesis of mesoporous NiO/Bi_2WO_6 nanocomposite for selective oxidation of alcohols. *Solid State Sci.* **2020**, *107*, 106306.

(6) Adil, S. F.; Assal, M. E.; Shaik, M. R.; Kuniyil, M.; Hashmi, A.; Khan, M.; Khan, A.; Tahir, M. N.; Al-Warthan, A.; Siddiqui, M. R. H. Efficient aerial oxidation of different types of alcohols using ZnO nanoparticle-$MnCO_3$-graphene oxide composites. *Appl. Organomet. Chem.* **2020**, *34*, No. e5718.

(7) Ragupathi, C.; Judith Vijaya, J.; Narayanan, S.; Jesudoss, S.; John Kennedy, L. Highly Selective Oxidation of Benzyl Alcohol to Benzaldehyde with Hydrogen Peroxide by Cobalt Aluminate Catalysis: A Comparison of Conventional and Microwave Methods. *Ceram. Int.* **2015**, *41* (2), 2069−2080.

(8) Assal, M. E.; Shaik, M. R.; Kuniyil, M.; Khan, M.; Kumar, J. V. S.; Alzahrani, A. Y.; Al-Warthan, A.; Al-Tamrah, S. A.; Siddiqui, M. R. H.; Hashmi, A.; et al. Silver-doped manganese based nanocomposites for aerial oxidation of alcohols. *Mater. Express* **2018**, *8* (1), 35−54.

(9) Villa, A.; Wang, D.; Su, D. S.; Prati, L. New challenges in gold catalysis: bimetallic systems. *Catal. Sci. Technol.* **2015**, *5* (1), 55−68.

(10) Liu, Y.; Zhang, J.; Guan, H.; Zhao, Y.; Yang, J.-H.; Zhang, B. Preparation of bimetallic Cu-Co nanocatalysts on poly (diallyldimethylammonium chloride) functionalized halloysite nanotubes for hydrolytic dehydrogenation of ammonia borane. *Appl. Surf. Sci.* **2018**, *427*, 106−113.

(11) Shinde, V. M.; Skupien, E.; Makkee, M. Synthesis of Highly Dispersed Pd Nanoparticles Supported on Multi-Walled Carbon Nanotubes and Their Excellent Catalytic Performance for Oxidation of Benzyl Alcohol. *Catal. Sci. Technol.* **2015**, *5* (8), 4144−4153.

(12) Li, Z.; Li, H.; Yang, Z.; Lu, X.; Ji, S.; Zhang, M.; Horton, J. H.; Ding, H.; Xu, Q.; Zhu, J.; et al. Facile Synthesis of Single Iron Atoms over MoS_2 Nanosheets via Spontaneous Reduction for Highly Efficient Selective Oxidation of Alcohols. *Small* **2022**, *18* (19), 2201092.

(13) Khan, M.; Tahir, M. N.; Adil, S. F.; Khan, H. U.; Siddiqui, M. R. H.; Al-warthan, A. A.; Tremel, W. Graphene based metal and metal oxide nanocomposites: synthesis, properties and their applications. *J. Mater. Chem. A* **2015**, *3* (37), 18753−18808.

(14) Zhu, S.; Wang, J.; Fan, W. Graphene-based catalysis for biomass conversion. *Catal. Sci. Technol.* **2015**, *5* (8), 3845−3858.

(15) Yin, Z.; Liu, X.; Wu, F.; Lu, B.; Huang, B.; Chen, Y.; Lin, G. Fabrication of P-Doped Porous Carbon Catalysts, with Inherent N Functionality, from Waste Peanut Shells and Their Application in the Metal-Free Aerobic Oxidation of Alcohols. *ACS Sustainable Chem. Eng.* **2022**, *10* (2), 911−922.

(16) (a) Xu, C.; Dai, L.; Chen, Y.; Zhang, S.; He, C.; Wang, X. Enhanced interfacial interaction of mesoporous N, S co-doped carbon supported WO_3-WS_2 for green and selective oxidation of alcohols. *Appl. Surf. Sci.* **2023**, *609*, 155296. (b) Fiorio, J. L.; Garcia, M. A. S.; Gothe, M. L.; Galvan, D.; Troise, P. C.; Conte-Junior, C. A.; Vidinha, P.; Camargo, P. H. C.; Rossi, L. M. Recent advances in the use of nitrogen-doped carbon materials for the design of noble metal catalysts. *Coord. Chem. Rev.* **2023**, *481*, 215053.

(17) (a) Guan, H.; Liu, Y.; Bai, Z.; Zhang, J.; Yuan, S.; Zhang, B. Ag nanoparticles embedded in N-doped carbon nanofibers: a superior electrocatalyst for hydrogen peroxide detection. *Mater. Chem. Phys.* **2018**, *213*, 335−342. (b) Jia, Z.; Huang, F.; Diao, J.; Zhang, J.; Wang, J.; Su, D. S.; Liu, H. Pt NPs immobilized on a N-doped graphene@Al_2O_3 hybrid support as robust catalysts for low temperature CO oxidation. *Chem. Commun.* **2018**, *54* (79), 11168−11171.

(18) Hu, Z.; Zhou, G.; Xu, L.; Yang, J.; Zhang, B.; Xiang, X. Preparation of ternary Pd/CeO_2-nitrogen doped graphene composites as recyclable catalysts for solvent-free aerobic oxidation of benzyl alcohol. *Appl. Surf. Sci.* **2019**, *471*, 852−861.

(19) (a) Qiao, X.; Liao, S.; You, C.; Chen, R. Phosphorus and nitrogen dual doped and simultaneously reduced graphene oxide with high surface area as efficient metal-free electrocatalyst for oxygen reduction. *Catalysts* **2015**, *5* (2), 981−991. (b) Jeon, I. Y.; Zhang, S.; Zhang, L.; Choi, H. J.; Seo, J. M.; Xia, Z.; Dai, L.; Baek, J. B. Edge-selectively sulfurized graphene nanoplatelets as efficient metal-free electrocatalysts for oxygen reduction reaction: the electron spin effect. *Adv. Mater.* **2013**, *25* (42), 6138−6145.

(20) Wang, X.; Li, X.; Liu, D.; Song, S.; Zhang, H. Green synthesis of Pt/CeO_2/graphene hybrid nanomaterials with remarkably enhanced electrocatalytic properties. *Chem. Commun.* **2012**, *48* (23), 2885−2887.

(21) Ji, Z.; Shen, X.; Yang, J.; Zhu, G.; Chen, K. A novel reduced graphene oxide/Ag/CeO_2 ternary nanocomposite: green synthesis and catalytic properties. *Appl. Catal., B* **2014**, *144*, 454−461.

(22) Ramirez-Barria, C. S.; Isaacs, M.; Parlett, C.; Wilson, K.; Guerrero-Ruiz, A.; Rodríguez-Ramos, I. Ru nanoparticles supported on N-doped reduced graphene oxide as valuable catalyst for the selective aerobic oxidation of benzyl alcohol. *Catal. Today* **2020**, *357*, 8−14.

(23) (a) Assal, M. E.; Shaik, M. R.; Kuniyil, M.; Khan, M.; Alzahrani, A. Y.; Al-Warthan, A.; Siddiqui, M. R. H.; Adil, S. F. Mixed Zinc/ Manganese on Highly Reduced Graphene Oxide: A Highly Active Nanocomposite Catalyst for Aerial Oxidation of Benzylic Alcohols. *Catalysts* **2017**, *7* (12), 391. (b) Khan, M.; Adil, S. F.; Assal, M. E.; Alharthi, A. I.; Shaik, M. R.; Kuniyil, M.; Al-Warthan, A.; Khan, A.; Nawaz, Z.; Shaikh, H.; et al. Solventless Mechanochemical Fabrication of ZnO-$MnCO_3$/N-Doped Graphene Nanocomposite: Efficacious and Recoverable Catalyst for Selective Aerobic Dehydrogenation of Alcohols under Alkali-Free Conditions. *Catalysts* **2021**, *11* (7), 760.

(24) Assal, M. E.; Shaik, M. R.; Kuniyil, M.; Khan, M.; Al-Warthan, A.; Alharthi, A. I.; Varala, R.; Siddiqui, M. R. H.; Adil, S. F. Ag_2O nanoparticles/$MnCO_3$,-MnO_2 or-Mn_2O_3/highly reduced graphene oxide composites as an efficient and recyclable oxidation catalyst. *Arabian J. Chem.* **2019**, *12* (1), 54−68.

(25) Adil, S. F.; Assal, M. E.; Khan, M.; Shaik, M. R.; Kuniyil, M.; Sekou, D.; Dewidar, A. Z.; Al-Warthan, A.; Siddiqui, M. R. H. Eco-Friendly Mechanochemical Preparation of Ag_2O-MnO_2/Graphene Oxide Nanocomposite: An Efficient and Reusable Catalyst for the Base-Free, Aerial Oxidation of Alcohols. *Catalysts* **2020**, *10* (3), 281.

(26) Hummers, W. S.; Offeman, R. E., Jr. Preparation of Graphitic Oxide. *J. Am. Chem. Soc.* **1958**, *80* (6), 1339.

(27) Martínez-Prieto, L. M.; Puche, M.; Cerezo-Navarrete, C.; Chaudret, B. Uniform Ru nanoparticles on N-doped graphene for selective hydrogenation of fatty acids to alcohols. *J. Catal.* **2019**, *377*, 429−437.

(28) Zhao, Y.; Wu, D.; Chen, Y.; Li, Y.; Fan, X.; Zhang, F.; Zhang, G.; Peng, W. Thermal removal of partial nitrogen atoms in N-doped graphene for enhanced catalytic oxidation. *J. Colloid Interface Sci.* **2021**, *585*, 640−648.

(29) Wu, D.; Song, W.; Chen, L.; Duan, X.; Xia, Q.; Fan, X.; Li, Y.; Zhang, F.; Peng, W.; Wang, S. High-performance porous graphene from synergetic nitrogen doping and physical activation for advanced nonradical oxidation. *J. Hazard. Mater.* **2020**, *381*, 121010.

(30) Wang, Z.-l.; Xu, D.; Huang, Y.; Wu, Z.; Wang, L.-m.; Zhang, X.-b. Facile, mild and fast thermal-decomposition reduction of graphene oxide in air and its application in high-performance lithium batteries. *Chem. Commun.* **2012**, *48* (7), 976−978.

(31) Lerf, A.; He, H.; Forster, M.; Klinowski, J. Structure of graphite oxide revisited. *J. Phys. Chem. B* **1998**, *102* (23), 4477−4482.

(32) Srivastava, M.; Das, A. K.; Khanra, P.; Uddin, M. E.; Kim, N. H.; Lee, J. H. Characterizations of in situ grown ceria nanoparticles on reduced graphene oxide as a catalyst for the electrooxidation of hydrazine. *J. Mater. Chem. A* **2013**, *1* (34), 9792−9801.

(33) Cho, K. M.; Kim, K. H.; Park, K.; Kim, C.; Kim, S.; Al-Saggaf, A.; Gereige, I.; Jung, H.-T. Amine-functionalized graphene/CdS composite for photocatalytic reduction of CO_2. *ACS Catal.* **2017**, *7* (10), 7064−7069.

(34) Kadam, M. M.; Dhopte, K. B.; Jha, N.; Gaikar, V. G.; Nemade, P. R. Synthesis, characterization and application of γ-MnO_2/graphene oxide for the selective aerobic oxidation of benzyl alcohols to corresponding carbonyl compounds. *New J. Chem.* **2016**, *40* (2), 1436−1442.

(35) Saito, R.; Hofmann, M.; Dresselhaus, G.; Jorio, A.; Dresselhaus, M. Raman spectroscopy of graphene and carbon nanotubes. *Adv. Phys.* **2011**, *60* (3), 413−550.

(36) Sánchez-García, J.; Benito, A. M.; Maser, W. K.; García-Bordejé, E. Ru supported on N-doped reduced graphene oxide aerogels with different N-type for alcohol selective oxidation. *Mol. Catal.* **2020**, *484*, 110737.

(37) Kuniyil, M.; Kumar, J. V. S.; Adil, S. F.; Shaik, M. R.; Khan, M.; Assal, M. E.; Siddiqui, M. R. H.; Al-Warthan, A. One-pot synthesized Pd@ N-doped graphene: An efficient catalyst for Suzuki-Miyaura couplings. *Catalysts* **2019**, *9* (5), 469.

(38) Han, G.; Liu, Y.; Kan, E.; Tang, J.; Zhang, L.; Wang, H.; Tang, W. Sandwich-structured MnO_2/polypyrrole/reduced graphene oxide hybrid composites for high-performance supercapacitors. *RSC Adv.* **2014**, *4* (20), 9898−9904.

(39) Mahyari, M.; Shaabani, A. Graphene Oxide-Iron Phthalocyanine Catalyzed Aerobic Oxidation of Alcohols. *Appl. Catal., A* **2014**, *469*, 524−531.

(40) Xu, C.; Zhang, L.; An, Y.; Wang, X.; Xu, G.; Chen, Y.; Dai, L. Promotional synergistic effect of Sn doping into a novel bimetallic Sn-W oxides/graphene catalyst for selective oxidation of alcohols using aqueous H_2O_2 without additives. *Appl. Catal., A* **2018**, *558*, 26−33.

(41) Hu, Z.; Zhao, Y.; Liu, J.; Wang, J.; Zhang, B.; Xiang, X. Ultrafine MnO_2 nanoparticles decorated on graphene oxide as a highly efficient and recyclable catalyst for aerobic oxidation of benzyl alcohol. *J. Colloid Interface Sci.* **2016**, *483*, 26−33.

(42) Yang, Y.; Luo, L.-M.; Guo, Y.-F.; Dai, Z.-X.; Zhang, R.-H.; Sun, C.; Zhou, X.-W. In situ synthesis of PtPd bimetallic nanocatalysts supported on graphene nanosheets for methanol oxidation using triblock copolymer as reducer and stabilizer. *J. Electroanal. Chem.* **2016**, *783*, 132−139.

(43) (a) Gaffet, E.; Harmelin, M.; Singh, D. K.; Kesavamoorthy, R.; Panigrahi, B. K.; Nair, K. G. M. Correlation between microstructure and optical properties of ZnO nanoparticles synthesized by ball milling. *J. Appl. Phys.* **2007**, *102* (9), 093515. (b) Chakka, V. M.; Altuncevahir, B.; Jin, Z. Q.; Li, Y.; Liu, J. P. Magnetic nanoparticles produced by surfactant-assisted ball milling. *J. Appl. Phys.* **2006**, *99* (8), 08E912. (c) Gaffet, E.; Harmelin, M. Crystal-amorphous phase transition

induced by ball-milling in silicon. *J. Less-Common Met.* **1990**, *157* (2), 201−222.

(44) Yu, X.; Huo, Y.; Yang, J.; Chang, S.; Ma, Y.; Huang, W. Reduced Graphene Oxide Supported Au Nanoparticles as an Efficient Catalyst for Aerobic Oxidation of Benzyl Alcohol. *Appl. Surf. Sci.* **2013**, *280*, 450−455.

(45) Xie, X.; Long, J.; Xu, J.; Chen, L.; Wang, Y.; Zhang, Z.; Wang, X. Nitrogen-doped graphene stabilized gold nanoparticles for aerobic selective oxidation of benzylic alcohols. *RSC Adv.* **2012**, *2* (32), 12438−12446.

(46) Yang, X.; Wu, S.; Hu, J.; Fu, X.; Peng, L.; Kan, Q.; Huo, Q.; Guan, J. Highly efficient N-doped magnetic cobalt-graphene composite for selective oxidation of benzyl alcohol. *Catal. Commun.* **2016**, *87*, 90−93.

(47) Wu, G.; Wang, X.; Guan, N.; Li, L. Palladium on graphene as efficient catalyst for solvent-free aerobic oxidation of aromatic alcohols: Role of graphene support. *Appl. Catal., B* **2013**, *136−137*, 177−185.

(48) Feng, X.; Lv, P.; Sun, W.; Han, X.; Gao, L.; Zheng, G. Reduced graphene oxide-supported Cu nanoparticles for the selective oxidation of benzyl alcohol to aldehyde with molecular oxygen. *Catal. Commun.* **2017**, *99*, 105−109.

(49) Wu, S.; He, Q.; Zhou, C.; Qi, X.; Huang, X.; Yin, Z.; Yang, Y.; Zhang, H. Synthesis of Fe_3O_4 and Pt Nanoparticles on Reduced Graphene Oxide and Their Use as a Recyclable Catalyst. *Nanoscale* **2012**, *4* (7), 2478−2483.

(50) Darvishi, K.; Amani, K.; Rezaei, M. Preparation, characterization and heterogeneous catalytic applications of GO/Fe_3O_4/HPW nanocomposite in chemoselective and green oxidation of alcohols with aqueous H_2O_2. *Appl. Organomet. Chem.* **2018**, *32* (5), No. e4323.

(51) Jha, A.; Mhamane, D.; Suryawanshi, A.; Joshi, S. M.; Shaikh, P.; Biradar, N.; Ogale, S.; Rode, C. V. Triple nanocomposites of $CoMn_2O_4$, Co_3O_4 and reduced graphene oxide for oxidation of aromatic alcohols. *Catal. Sci. Technol.* **2014**, *4* (6), 1771−1778.

(52) Han, Q.; Guo, X.-X.; Zhou, X.-T.; Ji, H.-B. Efficient selective oxidation of alcohols to carbonyl compounds catalyzed by Ru-terpyridine complexes with molecular oxygen. *Inorg. Chem. Commun.* **2020**, *112*, 107544.

(53) Zhou, X.-T.; Ji, H.-B.; Liu, S.-G. Solvent-free selective oxidation of primary and secondary alcohols catalyzed by ruthenium-bis (benzimidazole) pyridinedicarboxylate complex using hydrogen peroxide as an oxidant. *Tetrahedron Lett.* **2013**, *54* (29), 3882−3885.

(54) Devari, S.; Deshidi, R.; Kumar, M.; Kumar, A.; Sharma, S.; Rizvi, M.; Kushwaha, M.; Gupta, A. P.; Shah, B. A. Osmium (VI) catalyzed chemoselective oxidation of allylic and benzylic alcohols. *Tetrahedron Lett.* **2013**, *54* (48), 6407−6410.

(55) Borthakur, R.; Asthana, M.; Kumar, A.; Lal, R. A. Cooperative Catalysis by Polymetallic Copper-Zinc Complexes in the Efficient Oxidation of Alcohols under Solvent Free Condition. *Inorg. Chem. Commun.* **2014**, *46*, 198−201.

(56) Assady, E.; Yadollahi, B.; Riahi Farsani, M.; Moghadam, M. Zinc Polyoxometalate on Activated Carbon: An Efficient Catalyst for Selective Oxidation of Alcohols with Hydrogen Peroxide. *Appl. Organomet. Chem.* **2015**, *29* (8), 561−565.

(57) Parmeggiani, C.; Cardona, F. Transition Metal Based Catalysts in the Aerobic Oxidation of Alcohols. *Green Chem.* **2012**, *14* (3), 547−564.

(58) Yang, Z.; Li, J.; Yang, X.; Xie, X.; Wu, Y. Gas-phase oxidation of alcohols over silver: The extension of catalytic cycles of oxidation of alcohols in liquid-phase. *J. Mol. Catal. A: Chem.* **2005**, *241* (1−2), 15−22.

(59) Kolobova, E. N.; Pestryakov, A. N.; Bogdanchikova, N.; Cortés Corberán, V. Silver catalysts for liquid-phase oxidation of alcohols in green chemistry: Challenges and outlook. *Catal. Today* **2019**, *333*, 81−88.

(60) Bailey, W. F.; Bobbitt, J. M.; Wiberg, K. B. Mechanism of the Oxidation of Alcohols by Oxoammonium Cations. *J. Org. Chem.* **2007**, *72* (12), 4504−4509.

(61) Sanderson, R. T. *Chemical Periodicity*; Springer: Reinhold, 1960.

(62) Waterhouse, G. I. N.; Bowmaker, G. A.; Metson, J. B. Mechanism and active sites for the partial oxidation of methanol to formaldehyde

over an electrolytic silver catalyst. *Appl. Catal., A* **2004**, *265* (1), 85−101.

(63) Furukawa, M.; Nishikawa, Y.; Nishiyama, S.; Tsuruya, S. Effect of alkali metal added to supported La catalysts on the catalytic activity in the gas-phase catalytic oxidation of benzyl alcohol. *J. Mol. Catal. A: Chem.* **2004**, *211* (1−2), 219−226.

(64) Panrod, C.; Themsirimongkon, S.; Waenkaew, P.; Inceesungvorn, B.; Juntrapirom, S.; Saipanya, S. Effect of noble metal species and compositions on manganese dioxide-modified carbon nanotubes for enhancement of alcohol oxidation. *Int. J. Hydrog. Energy* **2018**, *43* (35), 16866−16880.